I&EC research
Industrial & Engineering Chemistry Research
pubs.acs.org/IECR
Article

Ostwald Ripening Modulation by Organofluorine Additives in Rigid Polyurethane Foams

Cosimo Brondi, Thomas Mosciatti,* and Ernesto Di Maio*

Cite This: *Ind. Eng. Chem. Res.* 2022, 61, 14868−14880

ABSTRACT: In this study, we investigated the preservation mechanisms induced by the use of organofluorine additives (OFAs), at different contents on the foaming process of water−pentane blown rigid polyurethane and polyisocyanurate foams (PUFs and PIRFs). The morphological evolution was observed via optical observation and characterized in terms of average bubble size and bubble density. For both PUFs and PIRFs, the foaming process was formed by a two-stage mechanism, consistent with the bubble growth and degeneration. The first foaming stage was affected by combined bubble coalescence and Ostwald ripening (OR) in the case of PUFs, while coalescence only in the case of PIRFs. The second foaming stage was affected by only OR for all the PU and PIR formulations. Interestingly, it was revealed that OFAs can act with two possible mechanisms: (i) enhanced air bubble inclusion during the mixing stage and (ii) OR inhibition effect on the bubble degeneration. The dual function was related to the unique chemical structures of the OFAs, conferring a high dissolution capacity for the gas phase such as air bubbles included in the polymeric phase, in which they are insoluble. In particular, the OR inhibition was regulated by the addition of OFA that possibly induced two effects: (i) a reduction in system surface tension that mitigated the Laplace pressure and (ii) the incompatibility of OFA with the polymeric phase that remains confined within the air bubbles, leading the partial pressure of OFA to contribute together with the partial pressure exerted by the other solutes so that the pressure of the internal bubble counterbalances the pressures of Laplace and the reacting mixture. In addition, morphology features such as foam density, average bubble size, anisotropy ratio, and open cell content were also measured. Based on the results, we observed that OFAs efficiently reduced the average bubble sizes of both PUFs and PIRFs, with negligible effects on the foam density, weakening of the bubble walls, and orientation of the bubble distribution.

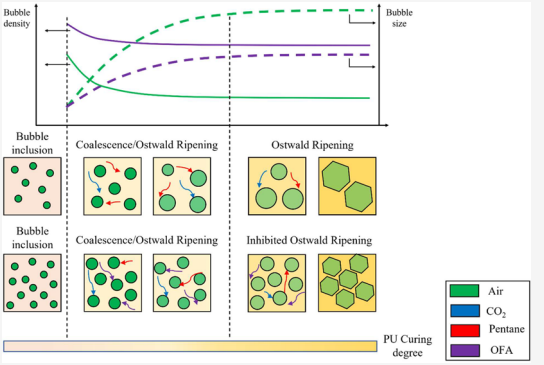

1. INTRODUCTION

Polymeric foams are two-phase systems in which a gas component is dispersed in a continuous polymeric matrix.[1] Among these materials, polyurethane foams (PUFs) are one of the most important classes due to their unique capacity to be tailored, flexible, or rigid, while combining tunable density with excellent mechanical and insulating properties.[2] Due to their outstanding versatility, PUFs are used in a multitude of different applications including automotive, furniture (cushioning materials), binders, thermal insulation, footwear, and household buildings.[3] The first urethane was synthesized in 1849 by Wurtz;[4] however, the first breakthrough was achieved by Otto Bayer in 1937 when he synthesized polyurethanes (PUs) from the reaction between a polyester diol and a diisocyanate.[4] In particular, rigid PUFs are typically prepared by vigorous mixing of polyol and isocyanate components under controlled conditions.[4] Blowing agents (BAs) and a variety of additives such as catalysts, surfactants, and, optionally, fire retardants are usually preblended into the polyol.[5] The formulated recipe is optimized to obtain a highly cross-linked and homogeneous rigid PU network, so that the final foam is characterized by good heat stability, high compression strength even at low density, and high barrier properties.[5]

Most of the reactions involved in the PU synthesis are exothermic, and the generated heat of reaction usually accomplishes the polymer curing.[5] The chemical complexity of PUs is due to the extreme reactivity of the isocyanate group (−N═C═O) toward the hydrogen active compounds, such as moieties containing the −OH and −NH functional groups.[5] In the polymerization process, often referred to as the *gelling reaction*, isocyanate and polyol react together to form the urethane group.[5] In the *blowing reaction*, the isocyanate reacts with water and gives as an initial product an unstable carbamic acid that spontaneously breaks down into carbon dioxide and a

Received: May 24, 2022
Revised: September 22, 2022
Accepted: September 22, 2022
Published: September 30, 2022

https://doi.org/10.1021/acs.iecr.2c01829
Ind. Eng. Chem. Res. 2022, 61, 14868−14880

primary amine. The corresponding amine can further react with another isocyanate molecule to give urea.[5] In the context of rigid PUFs, the gelling reaction causes the PU viscosity increase, while the generated gas (CO_2) from the blowing reaction acts as a chemical blowing agent (CBA) and provides the foam expansion. Appropriate catalysts are selected to tune the overall rates and balance these two reactions.[4,5] In the case of polyisocyanurate foams (PIRFs), additional catalysts can be selected to control also the *cyclotrimerization reaction* in which three isocyanates react together to give an isocyanurate ring.[5,6] As a result, a higher aromatic cross-linked network than that of PUFs is formed and confers to PIRFs an increased thermal stability and flame retardance.[5,7]

The PU reacting mixture typically undergoes a 30-fold increase in volume upon reaction with a further expansion driven by the difference between the internal gas bubble pressure and the external atmospheric pressure.[5] Complete expansion is achieved when the polymer has adequate strength to withstand the pressure difference or, in case of molded foams, once the mold is filled.[5] The morphology evolution during the foaming process has bubbles that first nucleate, grow, and then impinge and possibly merge into each other.[8−11] Bubble formation mechanisms can be aeration and nucleation. In *aeration*, the PU reactants are mixed by intense agitation that entraps air bubbles within the polymeric phase.[8] In *nucleation*, according to the classical nucleation theory (CNT),[9] the liquid/gas solution must overcome a thermodynamical (surface) energy barrier to let nucleation occur. In the present case, the limit is exceeded when the gas is supersaturated and precipitates in a form of metastable nuclei that may undergo growth beyond a critical radius or redissolution into the liquid matrix.[9] The so-generated bubbles (by nucleation and/or aeration) grow and can experience several different degeneration mechanisms such as drainage, coalescence, and Ostwald ripening.[10] *Drainage* is caused by capillary forces that transport the liquid material from the bubble walls toward the edge, called struts, resulting in thinner walls (Figure 1a). In *coalescence*, two bubbles approach each other (impingement) and can merge when the film thickness reaches a critical value (Figure 1b).[10] The *Ostwald ripening* (OR) occurs between two close bubbles presenting a significant difference in size and therefore different Laplace pressures. As a result, a mass transfer mechanism occurs, consisting in gas diffusion through the polymeric film from the smaller bubble to the bigger bubble, collapsing the smaller bubble until disappearance (Figure 1c).[10]

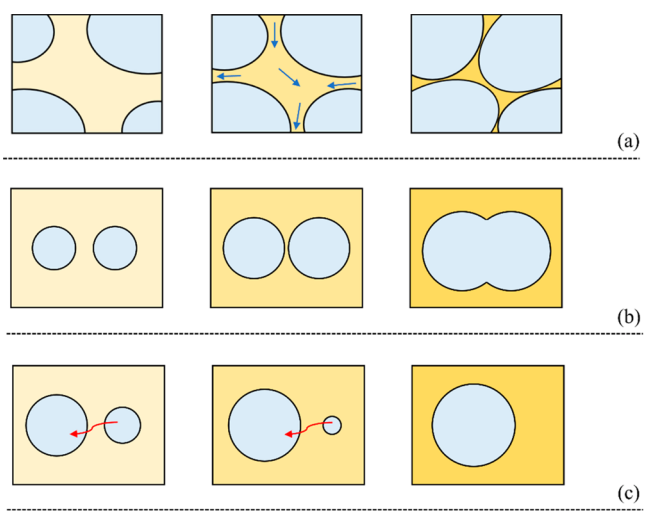

Figure 1. Scheme of bubble degeneration mechanisms taking place during the foaming process: (a) drainage, (b) coalescence, and (c) Ostwald ripening. Blue arrows indicate drainage flow, and red arrows indicate solute diffusion.

The balance between processing characteristics and the final properties is of paramount importance in development of rigid foams. The premise is even more entangled in the case of reacting materials. The key aspects in the processing are formulation composition, compatibility between components, and flow and reactivity of the reacting mixture, while for the final properties key elements are thermal conductivity, compression strength, density, and dimensional stability. These elements depend on the morphology features such as bubble size distribution, bubble density, volumetric fraction of open/closed bubbles, and solid fraction in the struts and walls. Several strategies have been explored to avail rigid foams with low thermal conductivity, achieved by producing fine and closed-cell foams.[5] One main approach consists in the introduction of additives into the PU overall recipe such as nonsoluble compounds and surface-active species that respectively promote bubble nucleation and stabilization. Nonsoluble additives can act as *nucleating agents* that, providing new interfaces partially available for bubble nucleation, induce a reduction of the surface energy barrier and favor heterogeneous nucleation.[5,9] Surface-active additives are commonly used in the PUF technology as *surfactants* with the dual role of promoting the mixing of incompatible components and reducing the surface tension of the available liquid/gas surfaces.[5,10] The approaches above presented rely on the use of surfactants designed on purpose or compositional changes of the bulk medium; however, the solute composition within the dispersed phase can also be driven to influence the gas diffusion through the liquid phase. The introduction of a incompatible species in the system (insoluble into the bulk phase) can limit the diffusion of soluble compounds. This approach was initially studied to stabilize liquid droplets in the case of emulsions.[12−15] For instance, Davis et al.[13] observed that OR was solely caused by a diffusive flux of dissolved solute molecules between two close droplets. The studied system was an emulsion with small droplets made of pure oil with a significant solubility in the continuous phase. The coarsening could be prevented by addition of molecules (or impurities such as electrolytes) that were insoluble into the continuous phase and hence were compatible with the oil droplets. The insoluble molecules (contained into the oil bubbles) provided an osmotic pressure counteracting the Laplace pressure (which drives OR), resulting in "osmotic stabilization". Later, the concept was further extended to the use of insoluble gases to stabilize liquid foams.[16] The addition of a gas characterized by a low compatibility or a gas mixture containing a trace of the insoluble species within the dispersed phase can slow the diffusion of a more soluble gas contained in the dispersed phase. As the soluble gas species progressively diffuse out the bubble, the insoluble species remains inside the bubble and increases its concentration, inducing a strong partial pressure which counteracts the Laplace pressure.[17] As an example, the OR could be significantly reduced by the use of insoluble compounds such as organofluorine additives (OFAs).[17] In their work, Bey et al.[18] reported the stabilization of gel foams by use of a gas mixture containing N_2 and insoluble perfluorohexane vapor. It was found that OR could be

https://doi.org/10.1021/acs.iecr.2c01829
Ind. Eng. Chem. Res. 2022, 61, 14868−14880

Table 1. Chemical Composition of Formulated Polyols

Chemicals	in PU formulation		in PIR formulation	
	Description	Parts	Description	Parts
Polyol formulation	VORACOR CW 7028	100	VORATHERM CN 1200	103
PBA	Cyclopentane	14.5 (11.5[a])	Cyclo/isopentane (70/30)	19.5 (16.5[a])
Other components	Water	0.1	Water	0.1
Liquid additive	HFB	0, 1, 2, 3	HFB	0, 1, 2, 3
	NFP	0, 1, 2, 3	NFP	0, 1, 2, 3

[a]When HFB or NFP content is greater than 0.

inhibited by a combined effect of gelation and the presence of an insoluble species within the gas bubbles that induced a partial pressure capable of withstanding the Laplace pressure. Moreover, they were able to discover that in the case of gel foaming systems the mechanism of stabilization is not only induced by an osmotic effect but rather a competition between the capillary pressure, elastic stresses in the gel, and osmotic pressure.

To the best of our knowledge, no study has been addressed so far on the use of liquid-type OFAs to inhibit OR in PUFs and PIRFs. Use of these types of additives for a specific PU formulation was reported in a patent application.[19] This work, introducing the "controlled inhibition of bubble Ostwald ripening" by use of OFAs in the context of rigid PUFs, is the follow up of previous works aimed at the fundamental understanding of the foaming mechanisms occurring during the PU foaming process and dealt with (1) the development of an inexpensive optical apparatus for processing and characterization of thermoset foaming materials,[20] (2) the investigation on the competing bubble formation mechanisms by a methodical approach that allowed one to separate bubble nucleation contribution from aeration,[20] (3) the measurement and modeling of the effect of air bubble inclusion on the PU reaction kinetics,[21] and (4) the characterization study of the OFA effect on the morphological properties as well as thermal conductivity and mechanical strength of PUFs and PIRFs.[22] The well-grounded studies allowed us to discern the different bubble degeneration mechanisms and surgically intervene on the OR, producing microcellular, low density PUFs (67 μm and 27.66 kg·m^{-3}), and PIRFs (40 μm and 32.78 kg·m^{-3}). The effects of two different liquid-type additives, namely, a partially perfluorinated compound such as "hexafluoro-2-butene" (HFB) and a fully perfluorinated compound such as "nonafluoro-4-(trifluoromethyl)-2-pentene" (NFP), have been investigated on two different PU and PIR formulations.

2. MATERIALS AND METHODS

2.1. Materials. A formulated mixture of polyether polyols (VORACOR CW 7028, OH number = 370, density = 1.08 g/cm^3, viscosity = 6700 mPa·s) and silicone surfactant and catalysts was utilized with polymeric methylene diphenyl diisocyanate (PMDI) (VORACOR CE 142, 31.1% NCO, 1.20 g/cm^3, 190 mPa·s) to produce PUFs. A formulated mixture of aromatic polyester polyols (VORATHERM CN 1200, OH number = 197, density = 1.24 g/cm^3, viscosity = 650 mPa·s) with silicone surfactant and catalysts was utilized with PMDI (high functionality) (VORACOR CE 620, 30.5% NCO, density = 1.24 g/cm^3, viscosity = 600 mPa·s) to produce PIRFs. All products were formulated and supplied by DOW Italia s.r.l. (Correggio, RE, Italy) and used "as received". All formulated polyols and isocyanate components implemented in this study can be purchased from DOW Europe GmbH (CH). Cyclopentane and a mixture of cyclo/isopentane (70/30) were used as physical blowing agents (PBAs) for PUFs and PIRFs, respectively (Synthesis S.p.A., Bianconese di Fontevivo, PR, Italy). The HFB and the NFP were supplied by Chemours (Turin, Italy) and 3M (Milan, Italy), respectively, and were used as liquid-type additives. Since HFB and NFP are very volatile, they were stored in a refrigerator before addition in the PU and PIR formulations. The chemical compositions of the formulated polyols used for the preparation of PUFs and PIRFs are reported in Table 1, while codes and mixing conditions for the different PU and PIR samples, together with the types and amounts of the used OFAs, are reported in Table 2.

Table 2. Foam Sample Codes with Types and Amounts of Water and OFAs

Sample	Water/OFA amount (parts)	Sample	Water/OFA amount (parts)	Mixing conditions
PU-neat	0.1/0	PIR-neat	0.1/0	1000 rpm (for 8 s)
PU-HFB-1	0.1/1	PIR-HFB-1	0.1/1	1000 rpm (for 8 s)
PU-HFB-2	0.1/2	PIR-HFB-2	0.1/2	1000 rpm (for 8 s)
PU-HFB-3	0.1/3	PIR-HFB-3	0.1/3	1000 rpm (for 8 s)
PU-NFP-1	0.1/1	PIR-NFP-1	0.1/1	1000 rpm (for 8 s)
PU-NFP-2	0.1/2	PIR-NFP-2	0.1/2	1000 rpm (for 8 s)
PU-NFP-3	0.1/3	PU-NFP-3	0.1/3	1000 rpm (for 8 s)

2.2. Optical Setup. A simple and inexpensive optical observation system, already reported in refs 20 and 21, has been setup and is shown in Figure 2. A high-speed camera (CMOS, model DMK 33UX178) from the Imaging source (Bremen, Germany) with a resolution of 3072 pixel × 2048 pixel (6.3 MP) and a frame rate of 60 fps has been used to collect microphotograms during the foaming process. The gain can be varied in the range of 0−48 dB, and each pixel has a size of 2.4 μm × 2.4 μm. A bitelecentric lens (model TC23004) from Opto Engineering (Mantova, Italy) was mounted (×2 magnification) with a working distance of 56 mm and a field depth of 0.23 mm. In the case of study of the PU and PIR foaming process and the OFAs effect on the OR inhibition, the reactants were poured in a sample holder and kept separate by a rubbery impeller, as shown in Figure 2c and d. When dealing with PUFs, polyol and isocyanate were mixed with a ratio of 1:1 by weight, while with PIRFs reactants were mixed with a ratio of 1:2 by weight. In both cases, the initial amount of polyol was 1 g, and mixing conditions were 1000 rpm for 8 s. The foaming process was readily observed right after the mixing stage. In the case of air bubble inclusion in the single phase (polyol or isocyanate), only one single reactant is poured in both the locations of the sample holder.

https://doi.org/10.1021/acs.iecr.2c01829
Ind. Eng. Chem. Res. 2022, 61, 14868−14880

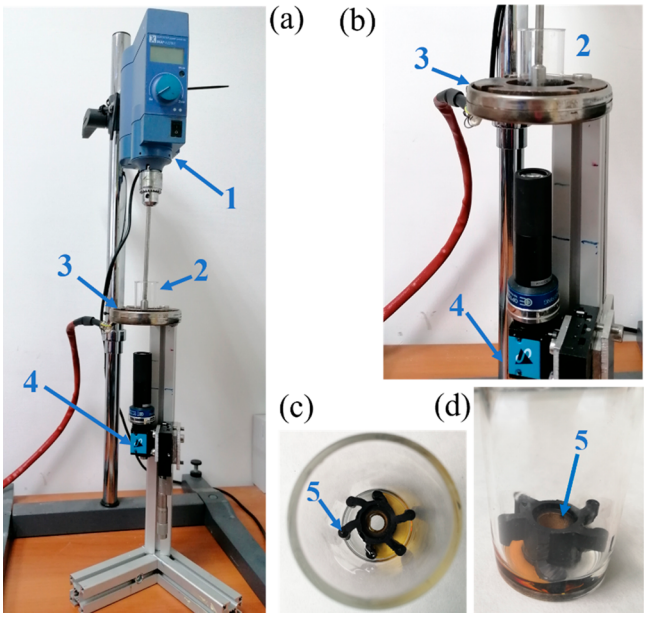

Figure 2. (a) Optical setup composed of (1) mixing head, (2) sample holder, (3) copper plate used to keep the sample holder, and (4) high-speed camera. (b) Detailed view of the optical camera coupled with the sample holder. (c) Top view of the sample holder with (5) the rubbery impeller keeping separate the two reactants before the mixing stage and (d) its frontal view.

2.3. Image Analysis. The morphology evolution of the different rigid foams was evaluated by a semiautomatic method of image analysis (IA) using ImageJ software (U.S. National Institutes of Health).[23] The region of interest (ROI), consisting in the selection of an area of interest of the image, was defined to conduct a more accurate analysis of the dispersed phases. As the final stage of the foaming process can still be characterized by a further expansion that contributes to cell wall thinning followed by subsequent wall drainage, we selected the ROI accordingly. In particular, the ROI was selected by identifying four bubbles at the four corners of a rectangular area, and different bubbles not undergoing degeneration were considered on the edges. In this way, the ROI uniformly moved and adapted to the foam growth, allowing one to decouple the observed OR from the bubble expansion. For both the analyses of the foaming process and the air bubble inclusion tests in the single reactant, the bubble diameter was defined as the diameter of a circle of area equivalent to the projected area of the dispersed phase and then multiplied by a correction factor of 1.273[24] to calculate the reference three-dimensional bubble size. The bubble density was evaluated by measuring the image area (A) and the number of the dispersed phases (n), according to Kumar's theoretical approximation.[25] In a fixed field of view, bubbles with a defined edge composed of a predefined range of low and high threshold values were taken into account for the evaluation of the bubble density, while bubbles with non-defined edges were considered out of the field and then not included in the parameter n. The height of the optical camera (as indicated in Figure 2) can be regulated so that several fields of view, starting from the bottom side of the sample holder, can be captured during the foaming process. In our case, in particular, the foaming process was observed in a field of view fixed at approximatively 200 μm of height starting from the bottom side.

The algorithm of the Canny edge detector, one of the most applied computational approaches first proposed by Canny[26] and then modified by Deriche,[27] was applied to detect the bubble candidate profiles. The IA was applied to 36 scans in the PU and PIR foaming process covering approximatively 300 s. Based on the selected ROI, average amounts of 220 and 320 bubbles were analyzed for PU and PIR formulations, respectively. For each formulation, the bubble size and the bubble density of three samples were measured and averaged.

2.4. Surface Tension Measurements. The surface tensions of the formulated polyols (supplied by DOW Italia s.r.l. and used "as received") were measured using the contact angle method. For each neat polyol and the polyol with its respective OFA, a single droplet was deposited on the flat surface of a glass plate. The contact angle between the droplet and the surface of the glass plate was then measured by using the ImageJ tool, and the liquid surface tension was calculated from eq 1[28]

$$\cos\theta = 2\phi\left(\frac{\gamma_S}{\gamma_{LV}}\right)^{1/2} - 1 \tag{1}$$

where θ is the contact angle, φ the ratio between the molar volumes of the liquid and solid phases, respectively, approximated to 1.0, γ_S the surface energy of the solid phase (24.8 mN/m for glass), and γ_{LV} the surface tension between the liquid and the vapor phases.[28] For each formulation, the surface tensions of three samples were measured and averaged.

2.5. Foam Characterization. *2.5.1. Foam Density.* Foam densities were measured according to ASTM D1622/D1622M-14 standard test method.[29] The foam was cured right after the foaming process at room temperature for 2 h. The sample was further cured at room temperature for at least 2 days before characterization. PU and PIR samples were cut using a razor blade and the size of each specimen was 10 mm × 10 mm × 10 mm (width × length × thickness). The densities of three samples were measured and averaged.

2.5.2. Scanning Electron Microscopy (SEM). The morphologies of the final PUFs and PIRFs were studied using scanning electron microscopy (SEM) with a PhenomXI microscope (PhenomWorld, Eindhoven, Netherlands), with a magnification range of 80−100,000× and a CeB_6 electron source tunable at 5.10 and 15 kV with a resolution of 14 nm. Specimens were cut with a razor blade and then coated with gold by a Quorum Q150AS (Quorum Technologies, Lewes, United Kingdom) rotary-pumped sputter. The average bubble size ($\overline{d}$) and the anisotropy ratio (AR) were evaluated according to the ASTM D3576-04 standard test method[24] using ImageJ.[23] The intersection method has been used to evaluate $\overline{d}$ by construction of a grid made of two perpendicular directions (m vertical lines of length h and n horizontal lines of length l). The grid is overlaid in each micrograph, and for each line, the number of bubbles intercepted is counted and the corresponding line (h or l) divided by the number of bubbles to obtain the bubble size of each line (d_i or d_j). For each formulation, the $\overline{d}$ and the AR of three samples are measured and averaged, according to eqs 2 and 3, respectively[30]

$$\overline{d} = \frac{\sum_{i=1}^{m} d_i + \sum_{j=1}^{n} d_j}{m + n} \tag{2}$$

https://doi.org/10.1021/acs.iecr.2c01829
Ind. Eng. Chem. Res. 2022, 61, 14868−14880

$$AR = \frac{\frac{\sum_{i=1}^{m} d_i}{m}}{\frac{\sum_{j=1}^{n} d_j}{n}} \quad (3)$$

2.5.3. Open Cell Content. The open cell (OC) content was measured by a pycnometer (Accupyc 1330, Micromeritics s.r.l., Milan, Italy) as described in ASTM D6226-14.[31] The OC contents of three samples were measured and averaged.

3. RESULTS AND DISCUSSION

3.1. Preliminary Considerations on Use of OFAs. At the beginning of this experimental study, we investigated under the idea that OFAs could induce a larger inclusion of air bubbles during the mixing step of the PU/PIR components. To investigate this hypothesis, an optical acquisition by high-speed camera was conducted on the polyether and polyester polyols (it was not possible to provide an acquisition for the isocyanate component as it was not suitable for optical observation). Air bubble inclusion tests were performed by mechanical stirring on the neat and the NFP polyols. Mixing speed was varied from 50 to 500 rpm, with a mixing time of 8 s. Based on an accurate choice of the ROI of interest, the air bubbles were counted taking into account 10 fields of view (each field was taken every 10 μm) starting from the bottom side of the sample holder. The same IA technique already described in Section 2.3 was used to detect the bubble candidate profiles. Figure 3 reports the average bubble size (a, c) and the number (b, d) of included air bubbles ($\overline{d_B}$ and n_B in the case of aeration on the single reactant) into the neat polyether polyol (PEP) and polyester polyol (PESP) with their respective HFB and NFP additions at three parts. The first observation is related to the increase in n_B with the mixing speed, occurring for each formulation. The rising trend can be ascribed to the dissipated kinetic energy provided from the dynamic mixer to the liquid medium that, at increasing rotation of the mixer, indisputably induces a larger gas/liquid surface capable of incorporating a larger air volume fraction.[32] The kinetic energy dissipation is an important parameter also in the regulation of the size distribution and the average size of the bubble population.[33] For each formulation, $\overline{d_B}$ reduces with the mixing speed as a consequence of the increasing shear stresses (standard deviation ranges from 1 to 3 μm for each experimental point). The higher the rotational speeds are of the mixing system, the stronger are the shear stresses exerted on the entrapped air bubbles.[34] Interestingly, for both the polyols, the OFA addition does not influence the observed trend of the reduction of the average size but induces a higher amount of included air bubbles of the liquid medium (standard deviations range from 4 to 7 for each experimental point). This behavior can be attributed to the unique properties of OFAs, including very high O_2 and N_2 solubilities.[35,36] OFAs are not capable of chemically interacting with gases due to their chemical structure. The high affinity for gases is derived from the extremely low polarizability of the fluorine−carbon bonds that results in low van der Waals interactions between OFA molecules.[37] These interactions are very weak intermolecular forces, in sharp contrast to their strong intramolecular bonds with gases of similar low cohesivity, such as O_2 and N_2.[38] Thus, the addition of liquid OFA to the neat polyol confers a higher gas dissolving capacity of the liquid system for air during the stirring stage.[39] A similar effect can be also deducted (and as will be observed) for the mixing stage of PUFs and PIRFs.

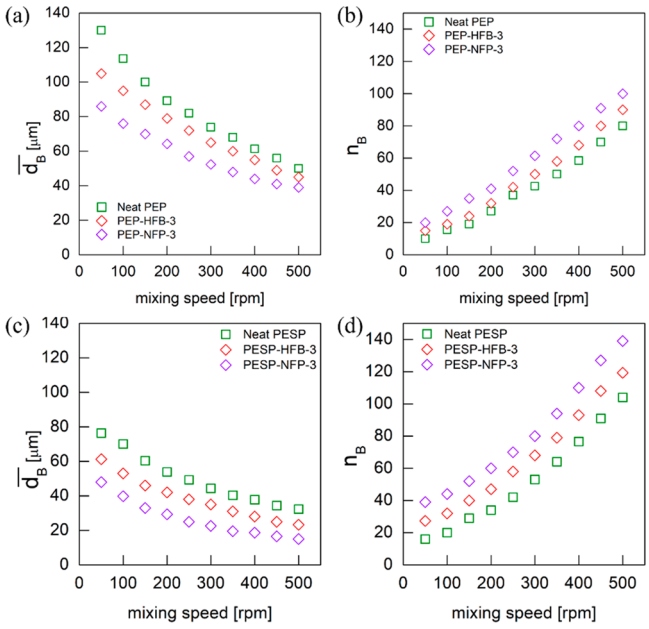

Figure 3. (a, c) Average bubble diameters. (b, d) Numbers of air bubbles included by mechanical stirring of neat polyether as well as polyester polyols with their respective HFB as well as NFP additions at three parts.

Further tests were performed on PU formulations in which no catalysts were included to provide a better understanding on the stabilization mechanism induced by OFA. Figure 4 reports the foaming process in the three following cases: (a) only silicone surfactant, (b) only NFP addition, and (c) addition of both additives, while Figure 5 reports these results

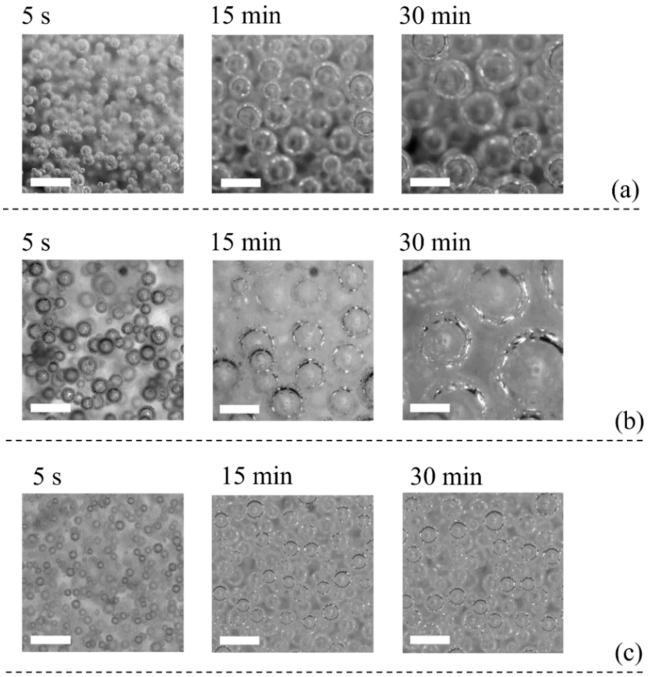

Figure 4. Photomicrographs of the PU foaming process (no catalyst addition) with (a) only silicone surfactant, (b) only NFP, and (c) silicone surfactant and NFP addition, respectively after 5 s and 15 and 30 min. Scale bars are 200 μm.

https://doi.org/10.1021/acs.iecr.2c01829
Ind. Eng. Chem. Res. 2022, 61, 14868−14880

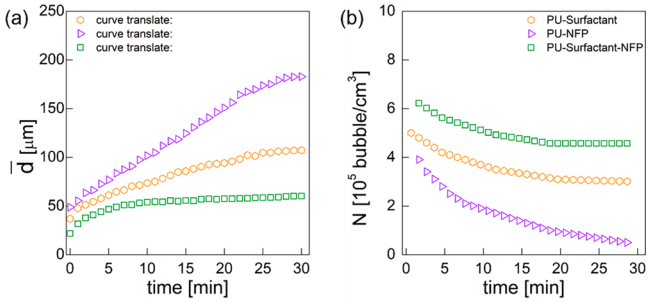

Figure 5. (a) Average bubble size and (b) average bubble density of the PU foaming process with no catalyst addition.

in terms of average bubble size ($\bar{d}$) and bubble density (N). In the first case (Figure 4a), a sample characterized by a coarser bubble size distribution than that obtained in the case of a PUF with an added catalyst was observed. The occurrence can be ascribed to an unbalanced competition between polymerization and a blowing reaction in which the polymer structure could not withstand bubble expansion.[21] After 30 min, a still ongoing PU foaming process was observed due to delayed reaction kinetics caused by the absence of catalyst within the PU recipe. On the contrary, when only NFP was added to the PU formulation, a dramatic coalescence was observed that affected the overall foaming process (Figure 4b). The bubble coalescence occurred also during the mixing step and during the early foaming stage. The OFA should induce a greater number of air bubbles included in the expanding system, but strong coalescence (caused by the absence of surfactant) dominated the aeration.[39] To fully exploit by which mechanism the OFA may possibly act on the inhibition of, we also calculated the surface tension between the polyol phase and the air phase from measurements of the contact angle of a sessile liquid droplet deposited on a flat surface. Figure 6

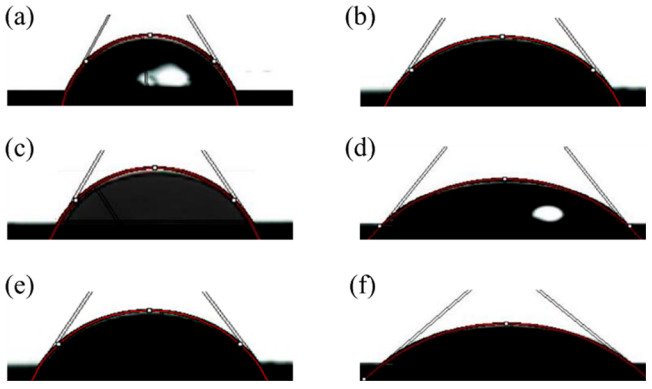

Figure 6. Contact angle measurements: (a, b) PEP and PESP neat materials, respectively, (c, d) PEP-HFB-3 and PESP-HFB-3, respectively, and (e, f) PEP-NFP-3 and PESP-NFP-3, respectively.

reports the images of the deposited droplets, and Table 3 reports the surface tension of neat materials (58.7 and 49.6 mN/m for PEP and PESP, respectively) and polyol formulations with their respective OFA added in three parts, namely, HFB (43.7 and 37.5 mN/m for PEP and PESP, respectively) and NFP (41.6 and 31.9 mN/m for PEP and PESP, respectively) mixtures. From these results, it can be observed that the addition of the OFA induces an effective

Table 3. Measurements of Surface Tension of Polyol Mixtures

Sample	Surface tension [mN/m]
PEP-neat	58.7 ± 2.2
PEP-HFB-3	43.7 ± 1.1
PEP-NFP-3	41.6 ± 0.5
PESP-neat	49.6 ± 2.7
PESP-HFB-3	37.5 ± 2.4
PESP-NFP-3	31.9 ± 0.8

reduction in surface tension compared to neat formulations, the effect being slightly more incisive when considering NFP.

It should be noted that a reduction in the surface tension reduction of the air/liquid interface can lead to an improved gas entrapment within the polymeric phase during the mixing stage.[33,34,40] Based on this occurrence, we can observe that the addition of the liquid OFA to the neat polyol results in more air bubbles included due to the synergic effect of a higher gas affinity of the liquid system for the air phase and reduced surface tension.

One can infer that the OFA does not intervene directly on the coalescence. A surfactant that acts on coalescence must rapidly adsorb to the available liquid/gas interfaces and possibly aggregate in the form of a monolayer (or multilayer) to compensate for the surface tension gradient and prevent wall thinning and subsequent collapse.[41] Although in several selected applications, the monolayer adsorption on a liquid/gas interface may also help in the OR inhibition, depending on the type of stabilizer and the solutes contained into the dispersed phase (nucleated BA bubbles or included air bubbles in case of PUFs).[42] Based on these observations, we can observe that the OFA can still intervene in the inhibition of the OR by only mitigation of the surface tension of the system that will reduce the Laplace pressure, governing the solubility of the solute species above high-curvature phase interfaces as described by the Kelvin effect.

In the third case (Figure 4c), it can be observed as the PUF is characterized by a finer bubble size distribution due to the synergic effect of both the additives. During the early foaming stage, the PU sample is characterized by a larger number of air bubbles than that of the first case, because of the enhanced affinity for the air phase induced by the OFA addition.[39] Moreover, these bubbles did not undergo a strong collapse since the mixing stage, due to the added silicon surfactant effect. Coalescence was the predominant bubble degeneration mechanism, and it was not possible to observe OR.

3.2. Ostwald Ripening Inhibition. Figure 7 depicts an example of the bubble morphology evolution during the (a) PU and (b) PIR foaming process in case of neat formulations and their corresponding HFB and NFP additions at three parts. From the initial microphotograms, a finer cellular structure can be noticed for the neat PIR formulation as a result of the different involved chemical mechanisms[5−7] as well as air bubble inclusion.[8,20,21] After 300 s from the mixing, the effect of the HFB on the morphology details is readily evident, translating in a reduced cellular structure and a more pronounced effect for the PIR formulation. Interestingly, the use of NFP induced a stronger effect than that of HFB. The PU-NFP-3 sample presents the finest cellular structure among the PU formulations, while PIR-NFP-3 is characterized by an average bubble size that spans several orders of magnitudes in comparison with the other two PIR formulations. From these

https://doi.org/10.1021/acs.iecr.2c01829
Ind. Eng. Chem. Res. 2022, 61, 14868−14880

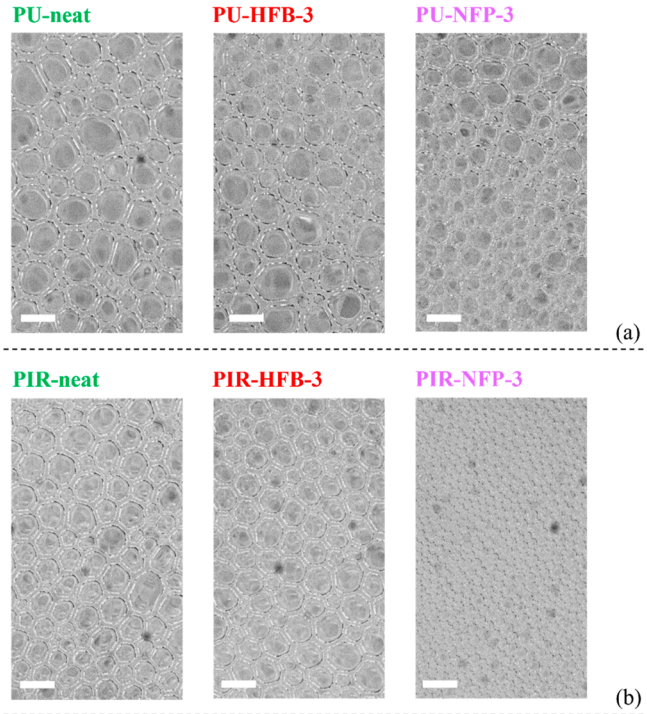

Figure 7. Photomicrographs of (a) PUFs and (b) PIRFs after 300 s. Scale bars are 200 μm.

observations, the first observation can consist in the production of a finer and more uniform (lower standard deviation) cellular structure of the foams when adding OFAs.

The foaming behavior of the several investigated formulations is reported in terms of average bubble size ($\overline{d}$) (standard deviation range from 10 to 15 μm for each experimental point) and bubble density (N) (standard deviation ranged approximatively from 2×10^3 to 4×10^3 bubble·cm^{-3} for each experimental point) in Figure 8 (PUFs) and Figure 9 (PIRFs). The first evidence emerges into the higher number on included

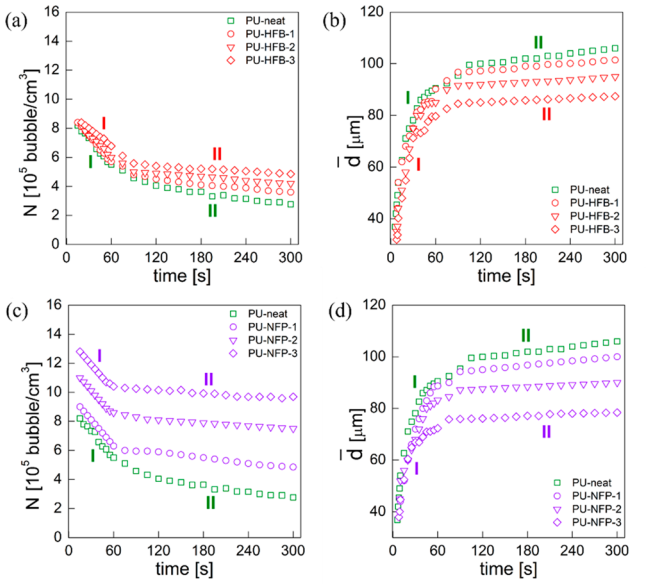

Figure 8. Average (a, c) bubble density and (b, d) bubble size of PUFs.

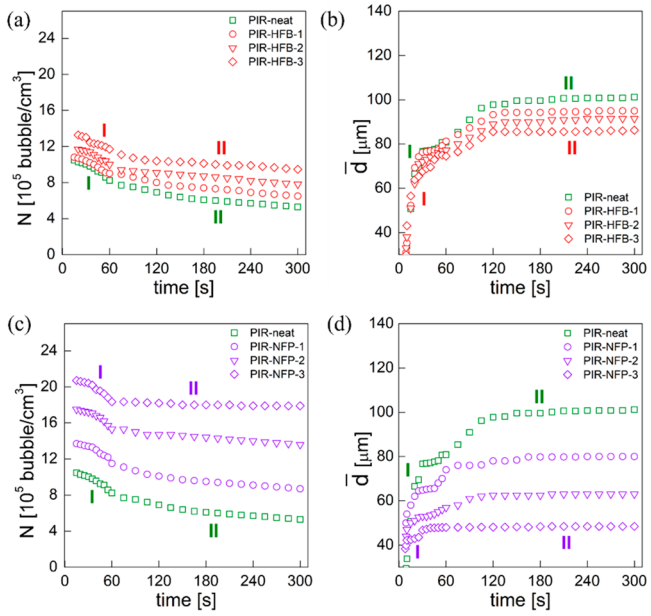

Figure 9. Average (a, c) bubble density and (b, d) bubble size of PIRFs.

air bubbles during the mixing stage when passing from neat formulations to those with additives, with this effect being more evident in the case of PIR formulations. As already investigated with the single corresponding polyols, this behavior can be attributed to the increased affinity for gases such as the air phase, induced by the unique chemical structure of the OFAs. Moreover, the NFP induced a stronger effect than that of HFB and can be related to the higher content of fluorine atoms contained in the molecular structure of these compounds.[35,36,38,39] The second major evidence, for all the formulations, consists in the foaming process characterized by two foaming stages. The first foaming stage (stage I) was characterized by a sharper change in N, while the second foaming stage (stage II) was characterized by a slighter decrease, depending on the strength and the type of degeneration mechanisms that affected the morphology evolution. In both foaming stages, we can observe no formation of new bubbles that could be attributed to nucleation, already observed in our previous works,[20,21] and it can be explained by the different levels of energy barriers that the gas/liquid system overcomes. In fact, gas molecules present in the reacting medium (CO_2 provided by blowing reaction, PBA and OFA evaporation), once supersaturated, would diffuse toward pre-existing air bubbles (included during the mixing stage) rather than nucleate due to no energy barrier to overcome.[43] Moreover, this circumstance is validated by the intrinsic property of OFA compounds that are completely incompatible with the polymer phase and, given the relative low boiling temperature, immediately evaporate during the foaming process and diffuse toward the dispersed phases.[35,37−39,43] The linear fitting of these experimental data provides a useful tool for the qualitative evaluation of the bubble degeneration rate (dN/dt)[44] (see Table 4). With reference to the PU formulations in stage I, we can observe that dN/dt decreases from −6261 to −4274 bubble·cm^{-3}·s^{-1} when passing from PU-neat to PU-HFB-3, respectively, and goes to −3938 bubble·cm^{-3}·s^{-1} in the case of PU-NFP-3. The

https://doi.org/10.1021/acs.iecr.2c01829
Ind. Eng. Chem. Res. 2022, 61, 14868−14880

Table 4. Apparent Diffusion Coefficients and Bubble Degeneration Rates of PUFs and PIRFs

	D_a[cm^2·s^{-1}]		dN/dt [bubble·cm^{-3}·s^{-1}]		Time intervals			Bubble degeneration mechanism	
Sample	I	II	I	II	I[a]	Transition[b]	II[a]	I	II
PU-neat	1.07 × 10^{-6}	6.26 × 10^{-8}	−6261	−800	(10−40 s)	(40−80 s)	(105−300 s)	Coalescence/OR	OR
PU-HFB-1	5.37 × 10^{-7}	9.42 × 10^{-10}	−6000	−622	(10−35 s)	(40−75 s)	(100−300 s)	Coalescence/OR	OR
PU-HFB-2	3.21 × 10^{-7}	4.36 × 10^{-10}	−5300	−476	(10−35 s)	(40−70s)	(90−300 s)	Coalescence/OR	OR
PU-HFB-3	1.47 × 10^{-7}	1.30 × 10^{-10}	−4274	−395	(10−30 s)	(40−60 s)	(90−300 s)	Coalescence/OR	OR
PU-NFP-1	4.32 × 10^{-7}	5.06 × 10^{-10}	−5867	−542	(10−35 s)	(40−65 s)	(90−300 s)	Coalescence/OR	OR
PU-NFP-2	2.27 × 10^{-7}	1.12 × 10^{-10}	−4765	−375	(10−30 s)	(40−60 s)	(90−300 s)	Coalescence/OR	OR
PU-NFP-3	7.23 × 10^{-8}	8.24 × 10^{-11}	−3938	−319	(10−30 s)	(35−60 s)	(80−300 s)	Coalescence/OR	OR
PIR-neat	2.76 × 10^{-7}	7.41 × 10^{-10}	−3170	−692	(10−25 s)	(50−80 s)	(150−300 s)	Coalescence	OR
PIR-HFB-1	2.72 × 10^{-7}	8.17 × 10^{-11}	−2860	−509	(10−25 s)	(50−80 s)	(135−300 s)	Coalescence	OR
PIR-HFB-2	2.75 × 10^{-7}	6.05 × 10^{-11}	−2864	−427	(10−25 s)	(45−80 s)	(135−300 s)	Coalescence	OR
PIR-HFB-3	2.69 × 10^{-7}	1.83 × 10^{-11}	−2856	−368	(10−25 s)	(45−80 s)	(120−130 s)	Coalescence	OR
PIR-NFP-1	2.70 × 10^{-7}	6.83 × 10^{-11}	−2815	−314	(10−25 s)	(40−75 s)	(130−300 s)	Coalescence	OR
PIR-NFP-2	2.72 × 10^{-7}	1.84 × 10^{-11}	−2802	−206	(10−25 s)	(40−75 s)	(125−300 s)	Coalescence	OR
PIR-NFP-3	2.68 × 10^{-7}	2.24 × 10^{-12}	−2806	−188	(10−25 s)	(40−75 s)	(90−300 s)	Coalescence	OR

[a]Time intervals in which procedures by eq 3 and linear fitting of N were applied. [b]Time interval in which transition from rounded to polyhedral bubbles was detected.

same observations can be conducted in the case of PIR formulations in stage I; dN/dt decreases from −3170 to −2856 bubble·cm^{-3}·s^{-1} when passing from PIR-neat to PIR-HFB-3 and goes to −2806 bubble·cm^{-3}·s^{-1} in the case of PIR-NFP-3. The first dN/dt reduction from neat to OFA formulations can be attributed to a combined effect of the reduced PBA amount and the inhibited OR. On one hand, a lower BA concentration may lead to lower dN/dt due to the depleted inflation into the air bubbles.[20,45] On the other hand, in the case of PUF, bubble growth in stage I was affected by coalescence and OR. The OFA presence leads to a reduced OR, and this effect can be assessed by the increasing OFA amount that progressively induces a minor OR and then a lower dN/dt. In the case of PIRFs, the dN/dt decreases from the neat to OFA formulations are related to the PBA decrease only. In fact, no OR was observed in PIR foaming stage I, and the increasing OFA amount does not induce a significant decrease in dN/dt.

All the investigated PU and PIR formulations were affected by only OR in foaming stage II. With reference to the PU formulations, dN/dt decreases from −800 to −395 bubble·cm^{-3}·s^{-1} when passing from PU-neat to PU-HFB-3, respectively, and goes to −319 bubble·cm^{-3}·s^{-1} in the case of PU-NFP-3. The same observations can be conducted in the cases of PIR formulations in stage I; dN/dt decreases from −692 to −368 bubble·cm^{-3}·s^{-1} when passing from PIR-neat to PIR-HFB-3, respectively, and goes to −188 bubble·cm^{-3}·s^{-1} in the case of PIR-NFP-3. The significant dN/dt decrease for both the formulations is related to the OFA that, once evaporated during the foaming process and being incompatible with the polymeric phase, establishes preferential paths toward the dispersed phases. In the case of the polyester polyol, as depicted in Figure 9, in both the emulsions large spherical bubbles are shown and correspond to air bubbles.

To further assess the initial state of the liquid mixture, Figure 10 reports some photomicrographs of air bubble inclusion conducted (at 100 rpm) on neat PESP and PESP-NFP-3 samples. It can be observed that, in the latter case, the polyol phase is covered with a large number of microdispersed phases, showing that the additive is not dissolved (being incompatible in the polyol phase), and due to the large difference in size, it can be clearly distinguished from air bubbles.

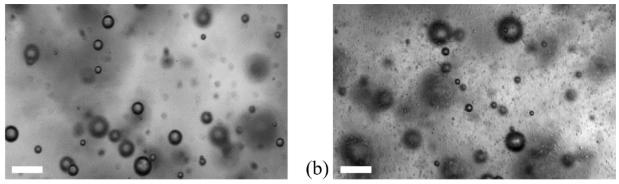

Figure 10. Photomicrographs of air bubble inclusion in the polyester polyol at 5 s right after the mixing step: (a) neat material and (b) NFB formulation. Scale bars are 100 μm.

As the foaming process progresses, the OFA remains confined into the air bubbles and contributes to the total internal bubble pressure exerted by the solutes. Thus, the air bubbles affected by OR stop decreasing in size, and the solutes (such as air, CO_2, cyclopentane, and cyclo/isopentane) do not diffuse out of the dispersed phases, while the partial pressure of the OFA increases and, together with the partial pressure of the other solutes, counterbalances the pressures of the Laplace and the reacting mixture, preserving the air bubble.[39] This effect is even more pronounced in the case of PIR formulations, corroborated by the increased amount of included air bubbles. This occurrence was already reported in a patent submitted by Klostermann et al.[19] In their work, the authors conducted the PU foaming without/with added organofluorine compounds in a high-pressure mixing head. Immediately after the exit from the mixing head, they analyzed 5 g of the reaction mixture in a Petri dish using a microscopy setup. Also in that case, they detected OR with no aging mechanisms related to coalescence. It is noteworthy that this was observed within 3 min after mixing of the PU components, consistent with the observed time scales in the context of this work. PUFs and PIRFs exhibited bubble size evolutions consistent with the two-stage foaming process observed in Figures 8a−c and 9a−c. The two-stage bubble growth was characterized by two linear trends that well fit the foaming stages I and II. Here, the observed bubble formation mechanism was provided by the air bubbles inclusion. These bubbles underwent growth caused by the inflation of the CBA/PBA as well as OFA molecules. After stage I, rounded air bubbles (wet regime) changed their shape into polyhedral and

https://doi.org/10.1021/acs.iecr.2c01829
Ind. Eng. Chem. Res. 2022, 61, 14868−14880

started to impinge (dry regime).[46] The bubble growth rate is then reduced, and a second linear trend (foaming stage II) was observed. To model this mass transport mechanism, as widely proposed in the literature,[44,47−50] a specific amount of liquid can be assigned to each individual air bubble in the liquid medium, and an average apparent diffusivity (D_a) can be defined by taking into account the mass flow of a plurality of components from the polymer matrix to the dispersed phase. Based on the average bubble size data acquired from the image sequences of the optical acquisition, we can extrapolate D_a, evidencing the reduction of diffusivity provoked by the ongoing curing reaction. The coefficient can be suitable determined by the following equation[51,52]

$$\bar{d} = 6\left(\frac{3}{4\pi}\right)^{0.33}(D_a t)^{0.5} \quad (4)$$

For each formulation (neat and with additives), when passing from stage I to stage II, a decrease in D_a can be noticed several orders of magnitude (Table 4). During stage I, polymeric chains of the thermosetting material are characterized by a higher degree of mobility that becomes more hindered and restricted due to the ongoing curing process (stage II). Therefore, the D_a reduction can be attributed to the reduced mobility of the solute species toward the dispersed phase.

The single bubble undergoing OR was monitored, and its dimension (different from the average bubble size evaluated on the overall bubble population) was calculated to provide a further hint of the inhibition mechanism induced by OFAs. Figures 11 and 12 report microphotograms of the bubble

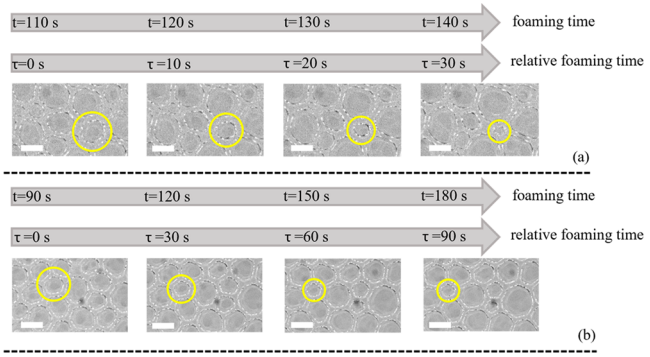

Figure 11. Photomicrographs of the foaming stage II of (a) PU-neat (t_{OR_0} = 110 s) and (b) PU-NFP-3 (t_{OR_0} = 90 s). The monitored bubble undergoing OR is reported in the yellow circle. Reported times refer to the beginning of the foaming process, right after the mixing stage. Scale bars are 100 μm.

morphology evolution in the cases of PUFs and PIRFs, respectively, in foaming stage II to discern the OR from the coalescence (observed together in foaming stage I in case of PUFs). The optical observation was conducted on smaller bubbles that experienced OR and close to bubbles undergoing growth and no further degeneration. As an example, Figure 11 reports a comparison between the (a) neat formulation and (b) that with the NFP addition at three parts. In the former case, it can be observed that the monitored bubble decreased in size until its collapse, while in the latter case the bubble underwent stabilization for the whole foaming stage after an initial reduction. The same behavior can be noticed in the case of PIRFs, reported in Figure 12a and b. By using the Canny−

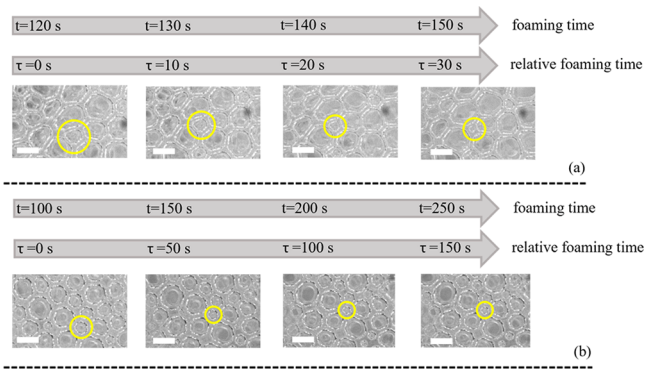

Figure 12. Photomicrographs of the foaming stage II of (a) PIR-neat (t_{OR_0} = 120 s) and (b) PIR-NFP-3 (t_{OR_0} = 100 s). The monitored bubble undergoing OR is reported in the yellow circle. Reported times refer to the beginning of the foaming process, right after the mixing stage. Scale bars are 100 and 50 μm, respectively.

Deriche algorithm for edge detection[26,27] and the intersection method,[24] it is possible to evaluate the time evolution of the diameter of the bubble undergoing OR, d_{OR}. Figure 13 reports

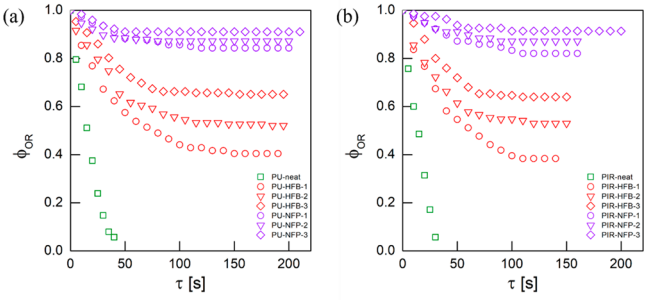

Figure 13. Size evolution of a single bubble undergoing OR in (a) PUFs and (b) PIRFs.

this evolution in terms of the normalized diameter, $\varphi_{OR} = d_{OR}/d_{OR_0}$, where d_{OR_0} is the bubble diameter at the beginning of the OR observation. A relative foaming time, $\tau = t - t_{OR_0}$, is utilized to shift the time at the beginning of the OR observation, where it is the initial time corresponding to the bubble that starts undergoing OR. For each PU and PIR formulation, the bubble sizes of 10 selected ROIs were calculated and averaged (standard deviation was approximatively between 2 and 4 μm for each sample). Figure 13 reports the normalized curves obtained for each formulation. Indeed, one can notice that the normalized bubble sizes of neat formulations do not approach a constant value but rapidly approach zero as the bubble undergoes deflagration. However, curves related to other formulations always reach their final value. On one hand, the time elapsed for φ_{OR} to attain its plateau and the shrinking rate decrease with the OFA amount, while the use of NFP translates in even higher plateau values at the end of foaming stage II. These results strengthen the observation that the OFA exerts a stabilizing action on those bubbles that may shrink and collapse due to established mass transfer mechanisms with close and bigger bubbles.

The use of organofluorine compounds for microbubble stabilization has been reported in the underlying literature.[53] Typically, the presence of a fluorine carbon bond in the molecular structure supports an extreme hydrophobicity (1

https://doi.org/10.1021/acs.iecr.2c01829
Ind. Eng. Chem. Res. 2022, 61, 14868−14880

order of magnitude higher than hydrocarbons) and confers a high volatility (due to their low intermolecular forces),[39] making these compounds suitable for air bubble stabilization. For instance, the stabilization of injectable dispersions of micrometer-sized organofluorine gas bubbles used as in vivo reflectors for contrast ultrasound imaging has been reported.[53] When bubbles containing water-soluble gases (i.e., O_2, N_2, and CO_2) are injected into circulation, these dissolve rapidly under the combined effect of blood pressure and Laplace pressure. However, the dissolution of these microbubbles can be prevented when OFAs are introduced into the system, and due to their poor water- olubility and high volatility, they tend to diffuse and remain inside the air bubbles leading to an equilibrium between the internal forces (partial pressures of the water-soluble gas and the OFA) and external forces (blood pressure and Laplace pressure). As is well known,[10,13,14,16,54] the driving force responsible for the OR is the difference in chemical potential of the solutes between the dispersed phase and the continuous phase, expressed by the so-called Kelvin effect

$$\Delta\mu = \mu(r) - \mu^{\infty} \cong \frac{2\sigma V_m}{r} \tag{5}$$

where $\mu(r)$ and μ^{∞} are, respectively, the solute chemical potentials of the dispersed phase and the continuous (bulk) phase, and r is the radius of the dispersed phase, σ the surface tension, and V_m the molar volume of the solute. Consequently, larger droplets (smaller curvature) are more energetically favored (minor difference between $\mu(r)$ and μ^{∞}) than smaller droplets (larger curvature). Therefore, there is a larger amount of solute molecules around smaller droplets, causing a solute concentration gradient from small to large droplets at the expense of the smaller ones.[54] The HFB and NFP additives have a high volatility and are incompatible in the polyol phase, and therefore, we may infer that, as the reaction proceeds, these additives evaporate due to the heat of reaction[10,13,14,16,54] and diffuse toward the included air bubbles. In the case of smaller bubbles, while the soluble and "more compatible" gases present inside (possibly air and BAs such as cyclopentane, cyclo/isopentane, and CO_2) diffuse out, the OFA concentration increases. As a consequence, the partial pressure of OFA increases and, combined with the partial pressure of the other solutes, which progressively reduce their diffusion out of the dispersed phases, counterbalance the Laplace and the reacting mixture pressures. Accordingly, the average apparent diffusion, obtained by evaluation of size distribution of the bubble population, can be used as a tool to further corroborate the observations made for a single shrinking bubble. The bubble shrinking decreases during the PU and PIR foaming lead to reduced molecular diffusion of the species contained in the reaction system, and their associated intermolecular movements can be adequately described by data related to D_a.[44,54,55] In fact, for the PUFs during foaming stage II, D_a goes from 6.26×10^{-8} to 9.42×10^{-10} $cm^2 \cdot s^{-1}$ for PU-neat and PU-HFB-1, respectively, and goes to 5.06×10^{-10} $cm^2 \cdot s^{-1}$ for PU-NFP-1 (Table 4). In the case of PIRFs, D_a goes from 7.41×10^{-10} to 8.17×10^{-11} $cm^2 \cdot s^{-1}$ for PIR-neat and PIR-HFB-1, respectively, and goes to 8.17×10^{-11} $cm^2 \cdot s^{-1}$ for PIR-NFP-1 (Table 4). These results evidence that the reduced shrinkage of the bubble (increased curvature) (Figure 11), due to the reduction in combined surface tension and the external forces (Laplace and reacting mixture pressures) counterbalanced by the partial pressures of the OFA and the other solutes, corresponds to a reduced apparent diffusion of these solute species.[44,54,55] Moreover, a significant effect of the increasing OFA content was also observed. For PUFs, D_a goes from 9.42×10^{-10} to 1.30×10^{-10} $cm^2 \cdot s^{-1}$ for PU-HFB-1 and PU-HFB-3, respectively, and goes from 5.06×10^{-10} to 8.24×10^{-11} $cm^2 \cdot s^{-1}$ for PU-NFP-1 and PU-NFP, respectively. In the case of PIRFs, D_a goes from 8.17×10^{-11} to 1.83×10^{-11} $cm^2 \cdot s^{-1}$ for PIR-HFB-1 and PIR-HFB-3, respectively, and goes from 6.83×10^{-11} to 2.24×10^{-12} $cm^2 \cdot s^{-1}$ for PIR-NFP-1 and PIR-NFP-3, respectively. From these results, it can be evidenced that a larger concentration of OFA molecules within the bubble can support a major contribution to the OFA partial pressure, exerting an enhanced stabilization mechanism on the bubble.[39] As discussed previously, the OR consists in a solute diffusive flux that establishes between a small and a big bubble, the latter becoming bigger at the expense of the smaller one. In the case of a liquid emulsion, and with no foam stabilizer, this would lead to complete disappearance of such a small bubble. As OFA acts on OR inhibition in the context of thermosetting PU foams, it can be considered that when the shrinking rate of the small bubble slows, the gelling reaction proceeds and a curing degree is achieved such that the bubble is "frozen" in the newly formed rigid structure. The combined results for D_a and φ_{OR} effectively confirmed that the OR is inhibited when OFAs are used, and their concentration is increased, leading to more contained big bubbles that did not grow at the expense of the smaller ones.

3.3. Foam Characterization. The morphologies of PUFs and PIRFs obtained with the neat formulation and the additives at three parts are shown in the SEM images reported in Figure 14. From the SEM micrographs, it was possible to measure the average bubble size and AR (Table 5). In addition, also results related to foam densities and OC content are provided. The cellular structure is finer and more uniform (lower standard deviation) when additives are used. On one hand, neat formulations are characterized by larger bubbles as a result of the combined coalescence and OR that affected the bubbles growth during foaming stage I and then OR only during foaming stage II. On the other hand, HFB and NFP formulations were characterized by a higher amount of included air bubbles due to the enhanced affinity for the air phase induced by OFAs, while these compounds also significantly inhibited the OR during the foaming process. As a result, the resulting foams were characterized by a more

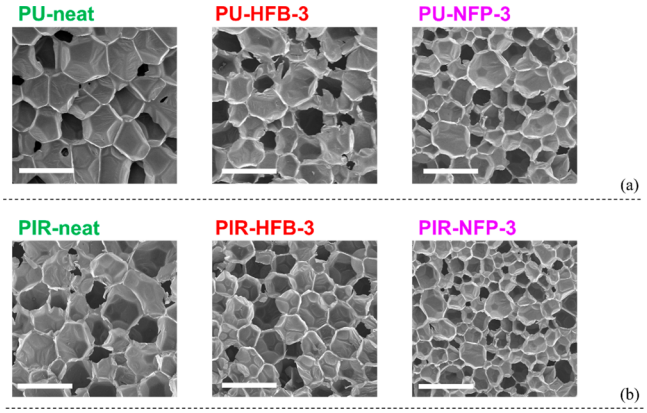

Figure 14. SEM micrographs of (a) PUFs and (b) PIRFs. Scale bars are 200 μm.

https://doi.org/10.1021/acs.iecr.2c01829
Ind. Eng. Chem. Res. 2022, 61, 14868−14880

Table 5. Morphological Features of PUFs and PIRFs

Sample	Foam density [kg·m^{-3}]	Average bubble size [μm]	AR	OC [%]
PU-Neat	28.2 ± 0.4	110 ± 18	1.02 ± 0.03	10.1 ± 0.1
PU-HFB-1	27.9 ± 0.3	103 ± 15	0.99 ± 0.06	10.2 ± 0.1
PU-HFB-2	27.7 ± 0.3	96 ± 13	1.04 ± 0.05	10.2 ± 0.2
PU-HFB-3	27.9 ± 0.2	89 ± 13	1.12 ± 0.04	10.1 ± 0.1
PU-NFP-1	27.9 ± 0.3	101 ± 16	1.09 ± 0.03	10.0 ± 0.1
PU-NFP-2	27.5 ± 0.3	87 ± 13	1.06 ± 0.05	10.1 ± 0.1
PU-NFP-3	27.7 ± 0.5	67 ± 12	1.08 ± 0.07	10.0 ± 0.2
PIR-Neat	33.4 ± 0.6	100 ± 15	0.98 ± 0.08	10.3 ± 0.1
PIR-HFB-1	32.8 ± 0.5	92 ± 13	1.02 ± 0.05	10.1 ± 0.1
PIR-HFB-2	32.6 ± 0.5	87 ± 12	1.04 ± 0.03	10.1 ± 0.2
PIR-HFB-3	32.7 ± 0.5	83 ± 12	1.10 ± 0.07	10.1 ± 0.1
PIR-NFP-1	32.8 ± 0.4	80 ± 10	1.06 ± 0.03	10.1 ± 0.1
PIR-NFP-2	32.5 ± 0.5	62 ± 9	0.92 ± 0.13	10.2 ± 0.2
PIR-NFP-3	32.8 ± 0.4	40 ± 9	0.92 ± 0.13	10.18 ± 0.24

homogeneous and finer bubble size distribution. This is in agreement with our previous study were we presented the general effect of the organofluorine additive on mechanical and morphological properties of bulk foams. Foam densities exhibited a slight reduction when additives were used. It can be attributed to further contribution of the OFAs that evaporate during the foaming process and led to a higher expansion ratio.[2,5,20] In this sense, OFAs appeared to not influence the foam density as they do not evidence a significant dependence on the increasing amount of liquid additives (Table 5). The AR, indicating the bubble orientation and deformation induced during the foaming process and then translated in elongated and oriented cellular structures of final foams,[5,8] indicate a negligible effect of the additives on the bubble orientation. Moreover, also results of the OC content indicate that the additives do not induce wall opening, differently from other foamed systems where solid-type functional nanofillers were added,[56] showing the advantages of additives in the liquid phase with respect to solid ones.

CONCLUSIONS

PU and PIR bubble growth and degeneration mechanisms were monitored via in situ micro-optical observation. The analysis of the images acquired by the optical camera allowed us to determine the average bubble size and the bubble density evolution with the curing time. Results revealed that the foaming process is formed by two stages: in the first stage, bubble growth was affected by combined coalescence and OR (coalescence only in case of PIRFs), while in the second stage OR was the only mechanism responsible for bubble degeneration.

The use of OFAs at increasing concentration in the PU/PIR foaming process induced a larger number of included air bubbles during the mixing stage of the reactants and significantly inhibited the bubble OR. The first mechanism was investigated by aeration tests on the single polyol components and both the PU and PIR formulations. The second mechanism was studied and modeled via apparent diffusivity of the solute molecules contained into the dispersed phases (air bubbles). We have shown for the first time how the high OFA affinity for the air phase and its relative incompatibility with the polymeric phase induces preferential diffusive paths of these species toward the air bubbles, with no bubble nucleation occurrence. The key bubble preservation phenomenon is possibly provided by two mechanisms: (i) reduction of the liquid/vapor surface tension and (ii) balance between the forces acting at the liquid/vapor interface, namely, OFA and the partial pressures of the other solutes, as well as the Laplace and reacting mixture pressures.

The resulting microstructures of PU and PIR samples were herein systematically studied. A direct relationship between the effect observed in the foaming phase and the final foam morphology was shown. Foams prepared with OFAs are characterized by finer and more uniform bubble size distributions, with a negligible effect of the OFA concentration on the foam density, anisotropy ratio, and open cell content. Microcellular thermosetting foams by using OFAs were achieved with average bubble diameters and foam densities of 67 μm and 27.66 kg·m^{-3} for PUFs and 40 μm and 32.78 kg·m^{-3} for PIRFs, respectively.

AUTHOR INFORMATION

Corresponding Authors

Thomas Mosciatti − *Polyurethanes R&D, DOW Italia s.r.l, 42015 Correggio, Italy;* orcid.org/0000-0003-2207-3246; Email: tmosciatti@dow.com

Ernesto Di Maio − *Dipartimento di Ingegneria Chimica, dei Materiali e della Produzione Industriale and foamlab, University of Naples Federico II, 80125 Naples, Italy;* orcid.org/0000-0002-3276-174X; Email: edimaio@unina.it

Author

Cosimo Brondi − *Dipartimento di Ingegneria Chimica, dei Materiali e della Produzione Industriale, University of Naples Federico II, 80125 Naples, Italy*

Complete contact information is available at: https://pubs.acs.org/10.1021/acs.iecr.2c01829

Notes

The authors declare no competing financial interest.

Biographies

Dr. Cosimo Brondi received his M.S. in chemical engineering from the University of Salerno, Italy, and his Ph.D. in industrial product and process engineering from the University of Naples Federico II, Italy. He is currently postdoc researcher in the Department of Chemical, Materials and Industrial Production Engineering, and his research focuses on the processing and modeling thermodynamics of mixtures of polymers and low molecular weight compounds. He is the recipient of the 2019 Raymond Shute Award of the Society of Plastics Engineers (Thermoplastic Materials & Foams Division).

https://doi.org/10.1021/acs.iecr.2c01829
Ind. Eng. Chem. Res. 2022, 61, 14868−14880

Dr. Thomas Mosciatti received a M.Sc. in Industrial Chemistry from University of Parma, Italy, and a Ph.D. in Chemistry from University of Strasbourg, France, under the supervision of Prof. Paolo Samorì. For his work on graphene in organic chemistry, he was awarded the Young Scientist Award by EMRS in 2015. In 2016, joined the iSwitch Marie Curie project developing holographic sensors for packaging, certified with the seal of excellence by the European Commission. In 2017, he joined DOW where he currently works as an associate scientist in the Polyurethanes R&D organization at the Dow PU Global Development Center in Correggio, Italy. He has authored 10 peer reviewed publications in international journals and has nine patent applications.

Dr. Ernesto Di Maio received his M.S. and Ph.D. in materials engineering from the University of Naples Federico II, Italy, where he is an associate professor in the Department of Chemical, Materials and Industrial Production Engineering. His research focuses on the processing and modeling of thermoplastic and thermosetting foams and on the physical properties of polymer/gas solutions relevant to foaming. He is the director of the foamlab, the Foaming Laboratory of the University of Naples, where new characterization and processing tools are developed to gain new understanding and to design new foamed materials and products. He is the recipient of the 2021 Morand Lambla Award of the Polymer Processing Society. He is an associate editor of the *Journal of Cellular Plastics*, SAGE Publishing Inc., a member of the Editorial Board of *Cellular Polymers*, SAGE Publishing Inc., and a member of the Editorial Board of the *Journal of Supercritical Fluids*, Elsevier B.V.

■ ACKNOWLEDGMENTS

The authors would like to thank Mr. Vanni Parenti, Mr. Luigi Bertucelli, Dr. Davide Micheletti, and Dr. Weijoun Zhou for useful discussions. Financial assistance from MIUR (PONRI 2014-2020) is gratefully acknowledged.

■ REFERENCES

(1) Jin, F.; Zhao, M.; Park, M.; Park, S. Recent Trends of Foaming in Polymer Processing: A Review. *Polymers* **2019**, *11*, 953.
(2) Guo, Q.Use of thermosets in the building and construction industry. In *Thermosets Structure, Properties, and Applications*, 2nd ed.; Elsevier: Amsterdam, The Netherlands, 2017; pp 279−300.
(3) Szycher, M.*Szycher's Handbook of Polyurethanes*, 2nd ed.; CRC Press: Boca Raton, FL, USA, 2012.
(4) Gama, N. V.; Ferreira, A.; Barros-Timmons, A. Polyurethane Foams: Past, Present, and Future. *Materials* **2018**, *11*, 1841.
(5) Randall, D.; Lee, S.*The Polyurethanes Book*, 1st ed.; Wiley: Hoboken, NJ, USA, 2003.
(6) Modesti, M.; Lorenzetti, A. An experimental method for evaluating isocyanate conversion and trimer formation in polyisocyanate-polyurethane foams. *Eur. Polym. J.* **2001**, *37*, 949−954.
(7) Singh, H.; Jain, A. K. Ignition, Combustion, Toxicity, and Fire Retardancy of Polyurethane Foams: A Comprehensive Review. *J. Appl. Polym. Sci.* **2009**, *111*, 1115−1143.
(8) Zhang, X. D.; Macosko, C. W.; Davis, H. T.; Nikolov, A. D.; Wasan, D. T. Role of silicone surfactant in flexible polyurethane foam. *J. Colloid Interface Sci.* **1999**, *215*, 270−279.
(9) Kashchiev, D.Thermodynamics of nucleation, Driving force for nucleation. In *Nucleation Basic Theory with Applications*; Butterworth-Heinemann: Oxford, UK, 2000, pp 9−16.
(10) Walstra, P. In *Fundamentals of Interface and Colloid Science*, Vol. *5*; Elsevier, Amsterdam, The Netherlands, 2005; pp 63−71.
(11) Cantat, I.; Cohen-Addad, S.; Elias, F.; Graner, F.; Höhler, R.; Pitois, O.; Rouyer, F.; Saint-Jalmes, A.; Cox, S.*Foams: Structure and Dynamics*, 1st ed.; Oxford University Press, Oxford, UK, 2013.
(12) Safouane, M.; Durand, M.; Saint Jalmes, A.; Langevin, D.; Bergeron, V. Aqueous foam drainage. Role of the rheology of the foaming fluid. *J. Phys. IV France* **2001**, *11*, Pr6-275−Pr6-280.
(13) Davis, S. S.; Round, H. P.; Purewal, T. S. Ostwald ripening and the stability of emulsion systems: an explanation for the effect of an added third component. *J. Colloid Interface Sci.* **1981**, *80*, 508−511.
(14) Webster, A. J.; Cates, M. E. Stabilization of Emulsions by Trapped Species. *Langmuir* **1998**, *14*, 2068−2079.
(15) Webster, A. J.; Cates, M. E. Osmotic Stabilization of Concentrated Emulsions and Foams. *Langmuir* **2001**, *17*, 595−608.
(16) Gandolfo, F. G.; Rosano, H. L. Interbubble Gas Diffusion and the Stability of Foams. *J. Colloid Interface Sci.* **1997**, *194*, 31−36.
(17) Weaire, D.; Pageron, V. Frustrated froth: evolution of foam inhibited by an insoluble gaseous component. *Philos. Mag. Lett.* **1990**, *62*, 417−421.
(18) Bey, H.; Wintzenrieth, F.; Ronsin, O.; Hohler, R.; Cohen-Addad, S. Stabilization of foams by the combined effects of an insoluble gas species and gelation. *Soft Matter* **2017**, *13*, 6816−6830.
(19) Klostermann, M.; Schiller, C.; Venzmer, J.; Eilbracht, C.Production of Fine Cell Foams Using a Cell Aging Inhibitor. World Patent WO2017093058A1, 2017.
(20) Brondi, C.; Di Maio, E.; Bertucelli, L.; Parenti, V.; Mosciatti, T. Competing bubble formation mechanisms in rigid polyurethane foaming. *Polymer* **2021**, *228*, 123877.
(21) Brondi, C.; Santiago-Calvo, M.; Di Maio, E.; Rodríguez-Perez, M. Á. Role of air bubble inclusion on polyurethane reaction kinetics. *Materials* **2022**, *15*, 3135.
(22) Brondi, C.; Di Maio, E.; Bertucelli, L.; Parenti, V.; Mosciatti, T. The effect of organofluorine additives on the morphology, thermal conductivity and mechanical properties of rigid polyurethane and polyisocyanurate foams. *J. Cell. Plast.* **2022**, *58*, 121−137.
(23) Abramoff, M. D.; Magalhaes, P. J.; Ram, S. J. Image Processing with Image. *J. Biophotonics Int.* **2004**, *11*, 36−42.
(24) *ASTM D3576-04: Standard Test Method for Cell Size of Rigid Cellular Plastics*; ASTM International: West Conshohocken, PA, USA, 2010.
(25) Kumar, V.Process Synthesis for Manufacturing Microcellular Thermoplastic Parts. Ph.D. Dissertation, Massachusetts Institute of Technology, Cambridge, MA, USA, 1988.

https://doi.org/10.1021/acs.iecr.2c01829
Ind. Eng. Chem. Res. 2022, 61, 14868−14880

(26) Canny, J. A Computational Approach to Edge Detection. *IEEE Trans. Pattern Anal. Mach. Intell.* **1986**, *PAMI-8*, 679−698.
(27) Deriche, R. Using Canny's criteria to derive a recursively implemented optimal edge detector. *Int. J. Comput. Vis.* **1987**, *1*, 167−187.
(28) Van Krevelen, D. W.; Te Nijenhuis, K.*Properties of Polymers: Their Correlation with Chemical Structure; Their Numerical Estimation and Prediction from Additive Group Contributions*; Elsevier, 2009.
(29) *ASTM D1622/D1622M-14: Standard Test Method for Apparent Density of Rigid Cellular Plastics*; ASTM International: West Conshohocken, PA, USA, 2014.
(30) Pinto, J.; Solórzano, E.; Rodriguez-Perez, M. A.; De Saja, J. A. Characterization of the cellular structure based on user-interactive image analysis procedures. *J. Cell. Plast.* **2013**, *49*, 555−575.
(31) ASTM International. *Standard test method for open cell content of rigid cellular plastics*; ASTM D6226-15; ASTI: West Conshohocken, PA, USA, 2021. DOI: 10.1520/D6226-21.
(32) Politova, N.; Tcholakova, S.; Valkova, Z.; Golemanov, K.; Denkov, N. D. Self-regulation of foam volume and bubble size during foaming via shear mixing. *Colloids Surf., A* **2018**, *539*, 18−28.
(33) Den Engelsen, C. W.; Isarin, J. C.; Gooijer, H.; Warmoeskerken, M. M. C. G.; Wassink, J. G. Bubble size distribution of foam. *Autex Res. J.* **2002**, *12*, 14−27.
(34) Kroezen, A. B. J.; Wassink, J. G. Bubble size distribution and energy dissipation in foam mixers. *J. Soc. Dyers Colour.* **1987**, *103*, 386−394.
(35) Castro, C. I.; Briceno, J. C. Perfluorocarbon-based oxygen carriers: review of products and trials. *Artif. Organs* **2010**, *34*, 622−634.
(36) Farris, A. L.; Rindone, A. N.; Grayson, W. L. Oxygen delivering biomaterials for tissue engineering. *J. Mater. Chem. B. Mater. Biol. Med.* **2016**, *4*, 3422−3432.
(37) Dalvi, V. H.; Rossky, P. J. Molecular origins of fluorocarbon hydrophobicity. *Proc. Natl. Acad. Sci. U. S. A.* **2010**, *107*, 13603−13607.
(38) Zhang, C.; Yan, K.; Fu, C.; Peng, H.; Hawker, C. J.; Whittaker, A. K. Biological utility of fluorinated compounds: from materials design to molecular imaging, therapeutics and environmental remediation. *Chem. Rev.* **2022**, *122*, 167−208.
(39) Riess, J. G. Understanding the Fundamentals of Perfluorocarbons and Perfluorocarbon Emulsions Relevant to In Vivo Oxygen Delivery. *Artif. Cells Blood Substit. Immobil. Biotechnol.* **2005**, *33*, 47−63.
(40) Deng, Q.; Anilkumar, A. V.; Wang, T. G. The role of viscosity and surface tension in bubble entrapment during drop impact onto a deep liquid pool. *J. Fluid Mech.* **2007**, *578*, 119−138.
(41) Rio, E.; Biance, A. Thermodynamic and Mechanical Timescales Involved in Foam Film Rupture and Liquid Foam Coalescence. *ChemPhysChem* **2014**, *15*, 3692−3707.
(42) Landers, R.; Modro, H.; Hubel, R.Influencing the cell structure of flexible polyurethane foams by additives In *Proceedings of the 2014 Polyurethane Technical Conference*, Dallas, TX, USA, 2014; pp 22−24.
(43) Jones, S. F.; Evans, G. M.; Galvin, K. P. Bubble nucleation from gas cavities—A review. *Adv. Colloid Interface Sci.* **1999**, *80*, 27−50.
(44) Pérez-Tamarit, S.; Solórzano, E.; Mokso, R.; Rodríguez-Perez, M. Á. In-situ understanding of pore nucleation and growth in polyurethane foams by using real-time synchrotron X-ray tomography. *Polymer* **2019**, *166*, 50−54.
(45) Wypych, G.Parameters of foaming In *Handbook of Foaming and Blowing Agents*; ChemTec Publishing, Toronto, Canada, pp 51−70, 2017.
(46) Furuta, Y.; Oikawa, N.; Kurita, R. Close relationship between a dry-wet transition and a bubble rearrangement in two-dimensional foam. *Sci. Rep.* **2016**, *6*, 1−8.
(47) Bird, R. B.; Stewart, W. E.; Lightfoot, E. N.*Transport Phenomena*, 2nd ed.; John Wiley & Sons: Hoboken, New Jersey, USA, pp 513−542, 2011.
(48) Patel, R. D. Bubble growth in a viscous Newtonian liquid. *Chem. Eng. J.* **1980**, *35*, 2352−2356.
(49) Amon, M.; Denson, C. D. A study of the dynamics of foam growth: analysis of the growth of closely spaced spherical bubbles. *Polym. Eng. Sci.* **1984**, *24*, 1026−1034.
(50) Favelukis, M.; Albalak, R. J. Bubble growth in viscous Newtonian and non Newtonian liquids. *Chem. Eng. J.* **1996**, *63*, 149−155.
(51) Campbell, G. M.; Mougeot, E. Creation and characterisation of aerated food products. *Trends Food Sci. Technol.* **1999**, *10*, 283−296.
(52) Baumhakel, R. Influence of stirring velocity and air loading on the formation of flexible urethane foams. *J. Cell. Plast.* **1972**, *8*, 304−310.
(53) Schutt, E. G.; Klein, D. H.; Mattrey, R. M.; Riess, J. G. Injectable microbubbles as contrast agents for diagnostic ultrasound imaging: the key role of perfluorochemicals. *Angew. Chem., Int. Ed.* **2003**, *42*, 3218−3235.
(54) Kabalnov, A. Ostwald ripening and related phenomena. *J. Dispersion Sci. Technol.* **2001**, *22*, 1−12.
(55) Al-Moameri, H.; Ghoreishi, R.; Suppes, G. Impact of inter- and intra-molecular movements on thermoset polymerization reactions. *Chem. Eng. Sci.* **2017**, *161*, 14−23.
(56) Laguna-Guterriez, E.; Hooghten, R. V.; Moldenaers, P. Effects Of Extrusion Process, Type And Content Of Clays, And Foaming Process On The Clay Exfoliation In HMS PP Composites. *J. Appl. Polym. Sci.* **2015**, *132*, 42828.